SimHumalator

A Human Radar Simulator

1. Working Principle of FMCW Radar

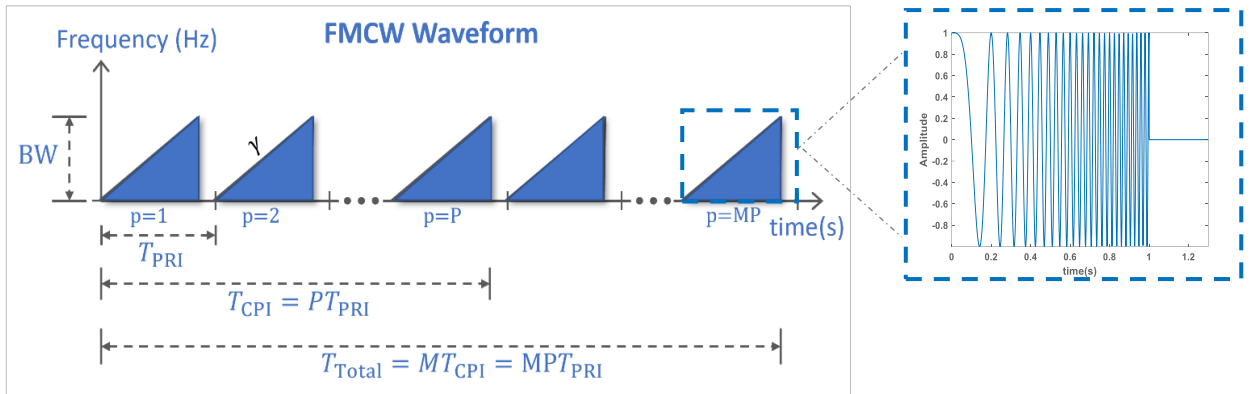A typical frequency modulated continuous wave (FMCW) radar waveform is shown in Fig.1.

Fig.1 A typical FMCW radar waveform

The transmitted waveform comprises of a sequence of linearly frequency modulated sinusoid waveforms (popularly known as chirps). The chirp is characterized by a carrier frequency (f_c), bandwidth (BW), the pulse repetition interval (T_{PRI}) and the duty cycle of the chirp. The duty cycle of the chirp determines the chirp duration (T_{CD}) within one pulse repetition interval (PRI). The remaining time is termed as the dead time when there is no signal. The transmit signal within one PRI can be mathematically represented as

$$y(t) = rect(\frac{t}{T_{PRI}})e^{j2\pi(f_c t + \frac{\gamma t^2}{2})} \tag{1}$$

Where, $rect(\frac{t}{T_{PRI}}) = \begin{cases} 1 & 0 \leq t \leq T_{CD} \\ 0 & T_{CD} \leq t \leq T_{PRI} \end{cases}$

The chirp factor $\left(\gamma = \frac{BW}{T_{CD}}\right)$, decides the rate at which the chirp ramps up or down. The sampling frequency (f_s) of the radar determines the number of samples in each T_{CD} also known as fast time samples. Let us assume the transmitted signal spans a duration T_{Total} consisting of M coherent processing intervals (CPIs). Each CPI in turn comprise of P PRIs. Therefore, the total number of PRIs in T_{Total} is MP PRIs.

The transmit sequence of chirps when falls upon the dynamic extended target (with B point scatterers) get backscattered. The backscattered signals are the complex sum of time-varying reflections from each of these scatterer. The reflections are simply attenuated (ρ_b), delayed (τ_b) and Doppler-shifted (f_{D_b}) version of the transmitted signal. The received signal within one CPI (slow time) can be represented as

$$y_r(t') = \sum_{b=1}^{B} \rho_b(t')y(t' - \tau_b - pT_{PRI})e^{-j2\pi f_{D_b} pT_{PRI}}, \tag{2}$$

where $t' \in [0, T_{CPI}]$

The delay in reflected signal is proportional to range of the target ($\tau_b = 2r_b(t')/c$), and phase difference between two consecutive chirps is proportional to the relative velocity between the radar and the target. The complex reflectivity $\rho_b(t')$, is proportional to the radar cross section of the target. We reformulate the above equation to present the received signal in baseband digitized form as

$$y_r[n,p] = \sum_{p=1}^{P} \sum_{b=1}^{B} \sigma_b[p]\, y(nt_s - \tau_b - pT_{PRI})e^{-j2\pi f_{D_b} pT_{PRI}} \qquad (3)$$

The pictorial representation of baseband digitized radar data is shown in Fig.2.

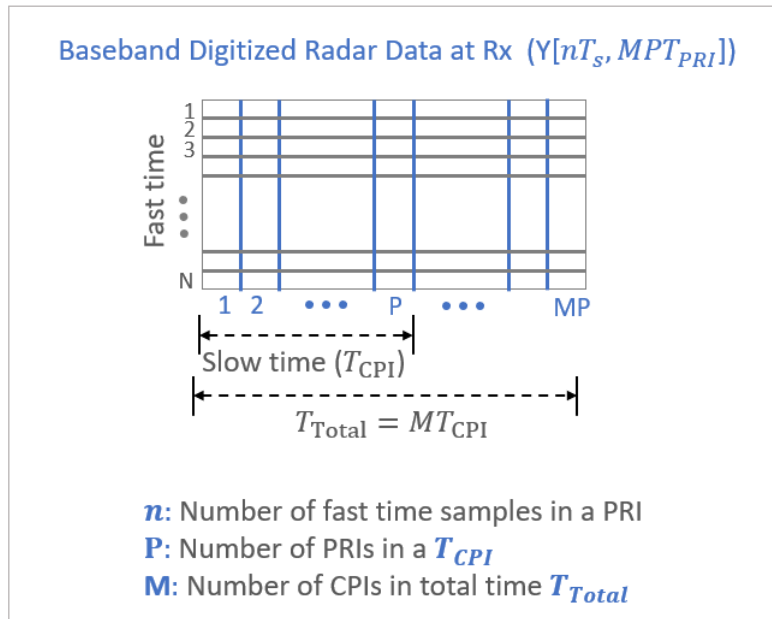

Fig.2 Baseband digitized received radar data

We process $y_r[n,p]$, two-dimensional received data through fast Fourier transforms (FFT) to obtain three radar signatures- high range resolution profiles, Doppler-time spectrograms and the range-Doppler ambiguity plots. We obtain high range resolution profiles by performing one-dimensional fast Fourier transform (FFT) over the fast time samples for each PRI and Doppler time spectrograms by performing short time Fourier transform (STFT) along the slow time as shown in Fig.3 and Fig.4 respectively.
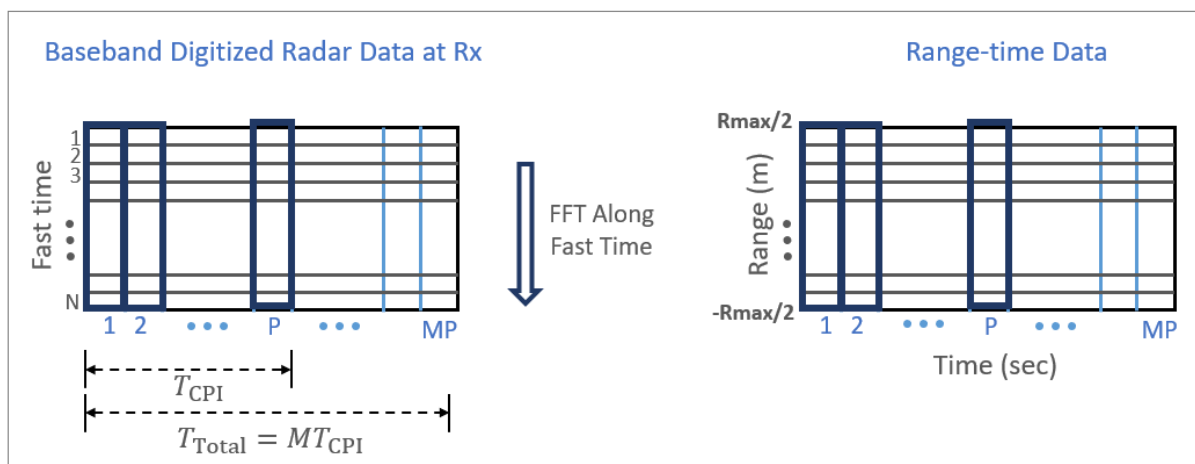

Fig. 3 High range resolution profile generation by performing FFT along fast time samples for each PRI
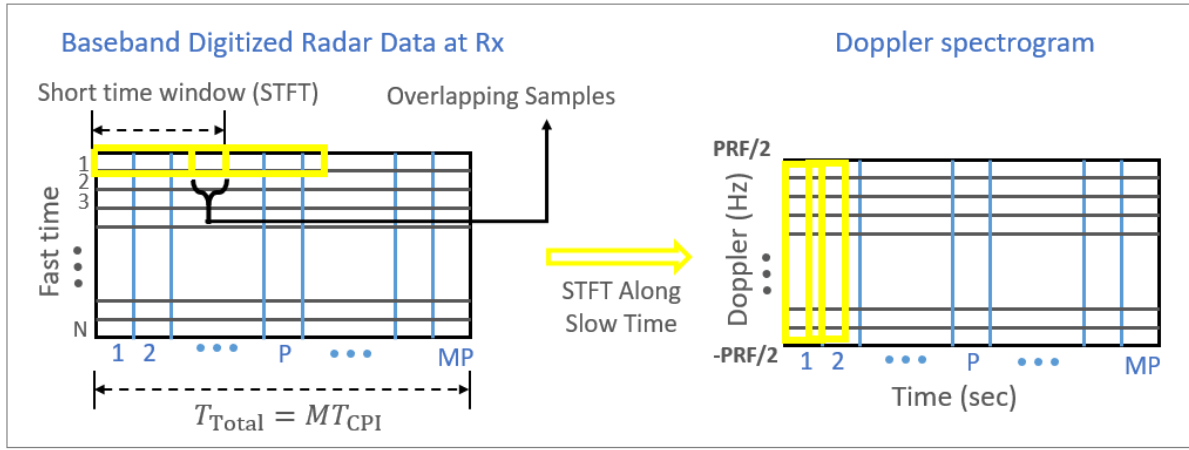
Fig. 4 Doppler-time spectrogram generation by performing FFT along slow time samples for each CPI

We perform two-dimensional fast Fourier transform (FFT) over the entire matrix shown in equation 3, to obtain the corresponding range-Doppler maps as shown in Fig.5.
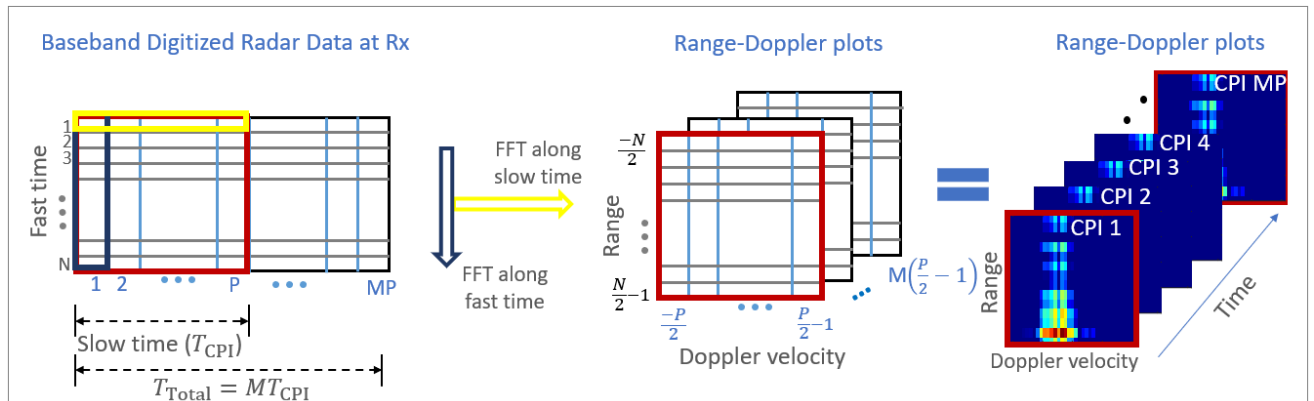

Fig.5 Range-Doppler maps generation by performing 2D-FFT along both fast time and slow time samples for each CPI

a. **Important points for deciding the simulation parameters**

    i. Range resolution is dictated by the bandwidth swept by the chirp

$$\Delta_r = \frac{c}{2BW}$$

    ii. Maximum range is limited by the ADC sampling frequency f_s

$$R_{max} = \frac{cf_s}{2\gamma}$$

    iii. Doppler resolution depends upon the coherent processing interval

$$\Delta_{f_D} = \frac{1}{T_{CPI}}$$

    iv. Maximum Doppler that can be detected is given by

$$f_{Dmax} = \pm \frac{PRF}{2}$$

$c = 3 \times 10^8$ m/s is the speed of light

$\gamma = \dfrac{BW}{T_{CD}}$ is the chirp factor

$PRF = \dfrac{1}{T_{PRI}}$ is the pulse repetition frequency

     b. Simulator simulate human radar returns as a function of following parameters-

         i. Radar Parameters
1. Radar Waveform Parameters
   a. Carrier frequency (Hz)
   b. Sampling frequency (Hz)
   c. Bandwidth (Hz)
   d. Pulse Repetition Frequency (PRF)
   e. Duty Cycle of Chirp
   f. Coherent Processing Interval (CPI)
2. Configuration of Radar
   a. Monostatic
   b. Bistatic Inline
   c. Bistatic Circular

         ii. Target Parameters
1. Activity type
2. File Number (Multiple files within each activity
3. Aspect angle of target with respect to radar
4. Initial location of target in space

         iii. Radar Signatures Generated
1. Baseband digitized radar returns
2. Range-Doppler Maps
3. Range-time Profiles
4. Doppler-time Profiles

References:

[1] S. S. Ram and H. Ling, "Simulation of human micro-Dopplers using computer animation data," in2008 IEEE Radar Conference.IEEE,2008, pp. 1–6.

[2] B. Erol and S. Z. Gurbuz, "A Kinect-based human micro-doppler simulator," IEEE Aerospace and Electronic Systems Magazine, vol. 30, no. 5, pp. 6–17, 2015.

[3] V. C. Chen, F. Li, S.-S. Ho, and H. Wechsler, "Analysis of micro-doppler signatures," IEEE Proceedings-Radar, Sonar and Navigation, vol. 150, no. 4, pp. 271–276, 2003.

[4] V. C. Chen, et. al, "Micro-doppler effect in radar: phenomenon, model, and simulation study," IEEE Transactions on Aerospace and electronic systems, vol. 42, no. 1, pp. 2–21, 2006

[5] Y. Deep, P. Held, S. S. Ram, D. Steinhauser, A. Gupta, F. Gruson, A. Koch, and A. Roy, "Radar cross-sections of pedestrians at automotive radar frequencies using ray tracing and point scatterer modelling," IET Radar, Sonar & Navigation, vol. 14, no. 6, pp. 833–844,2020.

[6] P. Held, D. Steinhauser, A. Kamann, T. Holdgrün, I. Doric, A. Koch, and T. Brandmeier, "Radar-based analysis of pedestrian micro-doppler signatures using motion capture sensors," in2018 IEEE Intelligent Vehicles Symposium (IV). IEEE, 2018, pp. 787–793.